Magnetoresistance oscillations in current-carrying high-T_c superconducting nano-loop networks

Omri J. Sharon

Department of Physics

Institute for Nanotechnology and Advanced Materials, Bar Ilan University

Ramat Gan 52115, Israel

(Dated: July 18, 2013)

PACS numbers:

Acknowledgements

First, I would like to thank Prof. Yosi Yeshurun and Prof. Avner Shaulov for their guidance and help. Since I was a freshman, I wanted to do my research in the field of superconductivity. Studing a quantum phenomenon in superconducting nano-structures made out of superconductor, fulfilled my expectations.

Secondly, I want to thank Dr. Ilya Sochnikov for teaching me almost everything I know about the e-beam lithography method and for the sample I used for my study.

I would also like to thank Daniel Levi and Tal Havdala for helping me whenever I needed his help, and for his counseling and company.

I gained much experience and knowledge at the University of Konstanz in Germany, and for that I would like to thank Prof. Elke Scheer and her group members, especially Christopher Espy.

Last but not least, I would like to thank my friends from Bar-Ilan university, especially Noam Haham who helped me more than I could ask, and collaborated with me in the theoretical study of my 'Fluxoid Network Dynamics'. To all of my friends at Bar-Ilan, thank you. This period of time wouldn't have been the same without you.

Contents

Abstract

This work extends a previous study of fluxoid quantization effects in high-T_c superconducting networks of nano-scale loops. Such networks were fabricated from atomically smooth Molecular Beam Epitaxially grown $La_{1.84}Sr_{0.16}CuO_4$ films. High resolution electron beam was used to prepare the pattern of thousands of loops made of 30 nanometer-wide wires.

Magnetoresistance measurements in such loops revealed periodic oscillations with a periodicity corresponding to the magnetic flux quanta, $\phi_0 = \frac{hc}{2e}$ (h is the Planck constant, c is the speed of light in vacuum and e is the electron's charge), as in the Little-Parks effect. However, the oscillations amplitude was larger by almost two orders of magnitude than the amplitude expected from the periodic changes in the critical temperature associated with the Little-Parks effect. Moreover, the amplitude of the oscillations showed a non-monotonic behavior exhibiting a peak at temperatures different than expected from the Little-Parks model.

To explain these results, Sochnikov *et al*. [Nature Nanotechnology 5, 516 (2010)] developed a dynamic model. This model ascribes the oscillations to the interaction of moving vortices in the wires with a periodic persistent current induced in the loops by the magnetic field.

The objective of the present work was to further examine this model by studying the dependence of the oscillations amplitude on the bias current. The experimental results show a non-monotonic dependence of the amplitude on the bias current which cannot be explained by the Little-Parks model.

In an effort to explain the results in the framework of the dynamic model of Sochnikov *et al*., we extended this model to include the effect of the bias-current based on the work of Tafuri and Kogan [Europhys. Lett. 73 948]. We show that the experimental results are consistent with the predictions of this extended model.

I. INTRODUCTION

A. Fluxoid Quantization

In 1948 London defined the term 'Fluxoid'[1] as:

$$\Phi' = \Phi + \frac{4\pi}{c} \oint_C \lambda^2 J \cdot dl \tag{1}$$

where $\Phi = \oint_c A \cdot dl = \iint_S B \cdot dS$ is the magnetic flux piercing a superconducting loop of circumference,C, c is the speed of light in vacuum, dl is the infinitesimal element of a path around the opening in the superconductor , λ is the magnetic field penetration depth and J is the super-current density. London predicted that in a multiply connected superconductor, the fluxoid, rather than the flux, is quantized. Namely, the fluxoid may have only discrete values and is quantized in units of superconducting flux quantum, Φ_0:

$$\Phi' = \Phi_0 n = n\frac{hc}{2e} \tag{2}$$

where n is an integer, h is the planck constant and e is the charge of the electron.

Several years later, this prediction was confirmed experimentally by Little and Parks [2–4] by measuring the magnetoresistance of a thin-walled superconducting cylinder. They found that the oscillations in the magnetoresistance had a period matching the magnetic flux quantum $\Phi_0 = hc/2e$.

An intuitive explanation for this effect is as follows: A Cooper pair should have the same order parameter $|\psi|^2$ after encircling the hole of the loop. The phase difference of the wave function ($\oint_C \nabla\varphi \cdot dl$) should be $2\pi n$ (n is an integer) so the wave function will be single-valued. However, applying magnetic field adds $\varphi_H = \frac{2e}{hc}\oint_C A \cdot dl$ to the phase [5], making the phase difference different from $2\pi n$. To satisfy the constraint of the $2\pi n$ phase difference, the superconductor applies super-currents that add another phase to the wave function so that the phase difference will be $2\pi n$.

For a single circular loop, isolating J from the fluxoid equation 1 yields:

$$J = \frac{\Phi_0 c\left(n - \frac{\Phi}{\Phi_0}\right)}{4\pi\lambda^2(2\pi r)} \tag{3}$$

where $2\pi r$ is the circumference of the loop.

Equation 3 predicts that the fluxoid current density is proportional to the inverse of the circumference. The kinetic energy associated with the fluxoid current density by Little and Parks is:

$$E_K = \frac{1}{2}Nmv^2 = \frac{1}{2}\frac{4\pi\lambda^2}{c^2}J^2 = \frac{\Phi_0^2 c\left(n-\frac{\Phi}{\Phi_0}\right)^2}{4\pi\lambda^2(2\pi r)^2} \tag{4}$$

where N is the number of the superelectrons, $2m$ is the mass and v is the average center of mass velocity of the cooper pairs. We assume that the integer is allowed to change in a way that keeps the kinetic energy minimized. As the external magnetic field H increases from zero, with $n = 0$, the kinetic energy increases quadratically with the magnetic flux. At $\Phi = \frac{1}{2}(hc/2e) = \frac{1}{2}\Phi_0$, n switches from 0 to 1, and a further increasing H results a decrease in the kinetic energy. At $\Phi = \frac{3}{2}\Phi_0$, n switches from 1 to 2, etc. Thus, the kinetic energy and the current are periodic with the flux with periodicity of hc/2e.

B. The Little-Parks model

The periodic kinetic energy is part of the free energy which determine the transition temperature, T_c, of the superconductor. In 1962, Little and Parks [2] suggested that the transition temperature T_c must be periodic with the flux piercing the loop, due to the dependence of T_c on the periodic kinetic energy of the superconductor.

The amplitude of the change in T_c was derived by Little and Parks [2]:

$$\Delta T_c = 0.14\frac{lE_f\hbar^2}{4mr^2\xi_0 k_B^2 T_c}\left(n-\frac{\Phi}{\Phi_0}\right)^2 \tag{5}$$

where l is the electronic mean free path, $\xi_0 = \hbar v_F/\pi\Delta$ is the Pippard coherence length, r the radius of the loop, m the electronic mass, and E_f the Fermi energy.

The periodic change in T_c causes a periodic change in the resistance measured near T_c and the connection between the two values can be approximated by:

$$\Delta R = \frac{dR}{dT}\Delta T_c \tag{6}$$

This equation tells us how much the resistance will change when T_c changes. When ΔT_c is the difference between the lowest and the highest critical temperatures, ΔR, is the oscillations amplitude in the magnetoresistance expected from Little-Parks model.

Magnetoresistance oscillations were observed in many studies [2–4, 6–16]. In most of these studies, the oscillations were studied as a function of temperature. A notable exception is the work of Berdiyorov and Peeters [9] who measured the oscillations in a 3 steps superconducting Niobium ladder in different bias currents and reported a change in the amplitude of the oscillations. However, they did not offer any model to explain their result.

In this study we present the first study of the dependence of the oscillations amplitude on the bias current in a network of superconducting nano-loops. We report a strong dependence of the oscillations amplitude on the bias current and compare our results with the predictions of both the Little-Parks and the fluxoid dynamic models.

C. The Fluxoid dynamic model

The Little-Parks model works well for low-T_c superconducting loops, but fails to explain the amplitude of the oscillations measured in the high-T_c loops [10–16]. To explain the experimental results in these materials, Sochnikov *et al*. [10] extended the fluxoid dynamics model [17] suggesting a new mechanism for magnetoresistance oscillations in high-T_c superconducting loops. In this theory the resistance in the loop is caused by vortices crossing the wire of the loop. Vortices have to overcome an energy barrier for crossing the wire and dissipate energy. This barrier has a strong dependence on the fluxoid currents . Because the fluxoid currents are periodic with the flux piercing the loop, the energy barrier is periodic with the flux as well. In other words, the periodic energy barrier causes oscillations in the magnetoresistance measurements.

This model does not take into account the dependence of the energy barrier on the bias-current. Since the bias currents contribute to the barrier energy [18], we expect the oscillations to be current dependent. The main objective of this research study is to investigate, both experimentally and theoretically, the dependence of the oscillations on the bias current.

D. Research objectives

- To measure the effect of bias-currents on the magnetoresistance oscillations at high-temperature superconducting networks.
- To extend the dynamic model to include the effect of bias currents on the magnetoresistance oscillations.
- To compare the experimental results with the predictions of the Little-Parks and the extended fluxoid dynamic models.

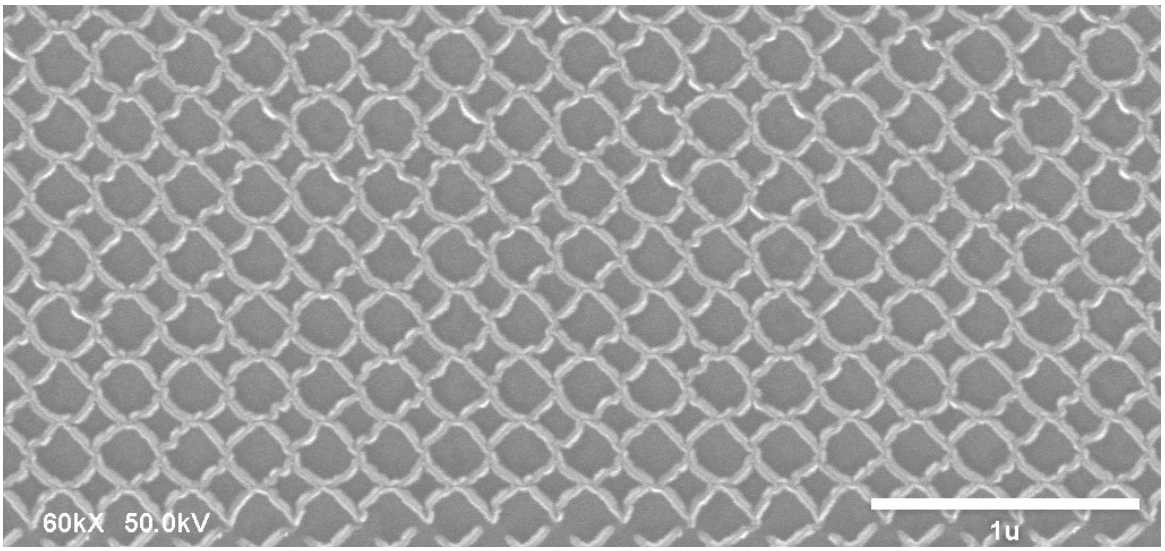

FIG. 1: Typical scanning electron microscope (SEM) image of part of the network measured in this study. The network consists of approximately 100x100 nm^2 and 200x200 nm^2 cells.

II. EXPERIMENTAL

Nano-loops were fabricated by Sochnikov [10–12] from high quality $La_{1.84}Sr_{0.16}CuO_4$ films grown by Molecular Beam Epitaxy. Using high-resolution electron beam writer, a mask of nano-loops was created on the layer of the electron beam resist. Then, the uncovered areas were etched by Ar-ion milling, leaving a pattern of $La_{1.84}Sr_{0.16}CuO_4$ nano-loops on STO substrate.
Figure 1 presents a typical scanning electron microscope (SEM) image of a part of the network composed of 100x100 nm^2 and 200x200 nm^2 loops.

The entire structure, including the contacts, is a single piece made of $La_{1.84}Sr_{0.16}CuO_4$ to avoid high contact resistance. The network resistance is then measured using a 4-point measurement methods. The bias-current is applied through two contact points and the voltage is measured between the other two. This structure is measured in a cryogenic system for transport measurements. In the following, we elaborate on the fabrication method and the experimental setup.

A. Films growth

The high quality $La_{1.84}Sr_{0.16}CuO_4$ films used in this study were grown at Brokhaven National Laboratory (BNL), in the group of Ivan Boovic,using a Molecular Beam Epitaxy (MBE) machine

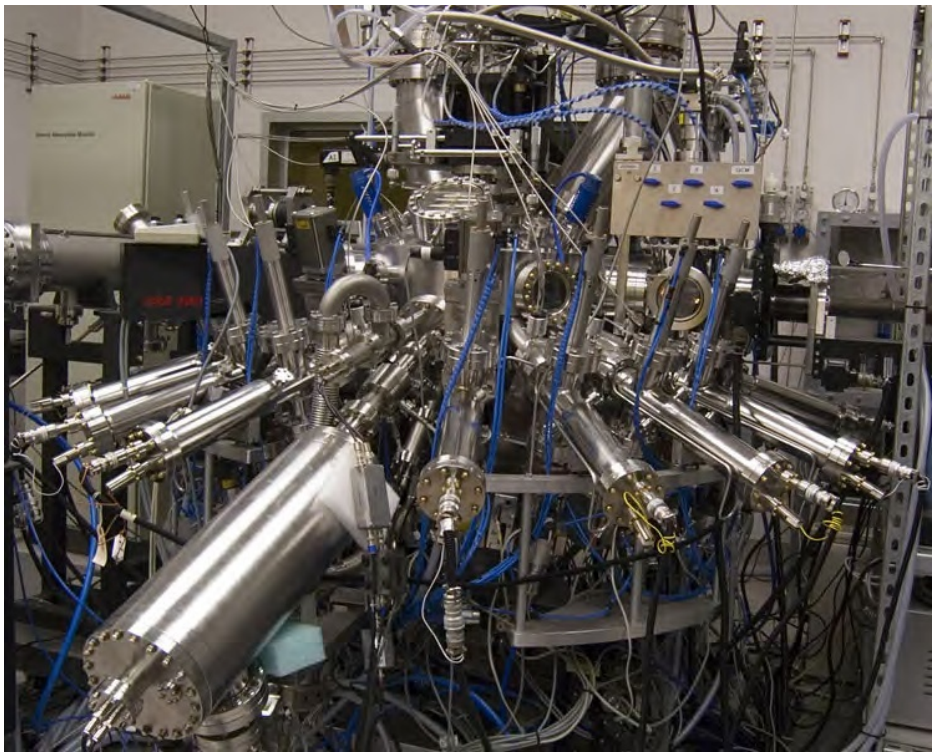

FIG. 2: Molecular Beam Epitaxy chamber at Brokhaven National Laboratory (Adapted from the Brookhaven Oxide MBE group website).

(figure 2). The deposition is preformed in ultra high vacuum ($< 10^{-8}\ Pa$), in a slow deposition rate that allows the film to be grown one atomic layer after the other in a controllable environment. Ultra-pure elements (La, Sr, Cu) are heated in separate cells until they begin to slowly evaporate (after melting or by sublimation). The gaseous elements then condense on the wafer, where they produce a layer of the desired compound.

The main tool at BNL is a unique multi-chamber Molecular Beam Epitaxy (MBE) system for the synthesis of complex oxides with atomic-layer precision.

A detailed description of the MBE system was described by Sochnikov in his Ph.D dissertation [19].

B. Nano patterning

A high resolution electron beam (e-beam) lithography system was exploited for nano-patterning the films. The e-beam system installed at the Bar-Ilan Institute of Nanotechnology and Advanced Materials is the CRESTEC-9000C (figure 3). The electron beam lithography is based on 'writing' with a focused electron beam in a thin layer of a material sensitive to the accelerated electrons (electron beam resist). The main advantage of electron beam lithography is that it is a very effective way to go beyond the diffraction limit of light and make features of few tens of nanometers or even less. In some cases, the exposed parts of the resist become highly soluble and can be removed by liquid developers (positive tone resists). In other cases, the exposed parts of the resist become unsolvable and the un-exposed parts can be removed by developers (negative tone resists).

We used Poly(methyl methacrylate) (PMMA) as a negative tone resist. Although, in typical conditions PMMA functions as a positive resist, at increased exposure times PMMA may crosslink and become unsolvable in typical organic developers [20]. We observed that a cross-linked negative tone PMMA ensures a much higher contrast, resolution, and aspect ratio. In a layer of 180 nm, we could reach an aspect ratio (width/height) of up to 1/10 in features down to 16 nm. Generally in thinner layers of PMMA, one can reach a resolution below 10 nm. Cross-linked PMMA are also very stable during ion milling, probably due to the enhanced stiffness of the crosslinked polymer.

The patterning steps are as follows:

1. Polymethyl methacrylate (PMMA) resist with a molecular weight of 495,000 (Microchem PMMA 495 A11) is diluted with anisole (approximately 50:50 volume ratio). This dilution ensures us a thin coating resist layer on top of our sample in reasonable spinning speeds.

2. After preparing the resist, we spin-coat the sample at a speed of 4,000 RPM to obtain a 180 nm thick layer of PMMA on top of our sample.

3. At this stage, the sample is 'baked' on a hot plate for 90 seconds at $180^{O}C$.

4. After coating the sample with a layer of resist, we expose the desired pattern using CRESTEC Cable-9000C high resolution e-beam lithography system with an acceleration voltage of 50 KeV and typical beam current of 1 nA.

5. Following this procedure is the contact exposure which is made the same way as the patterning exposure only in much higher beam current of 10 nA.

6. To remove parts of the resist near the negative unsolvable (cross-linked) parts of the PMMA, we sink the sample in a standard developer, based on MIBK (methyl isobutyl ketone). This 'negative' PMMA pattern served as a mask for the next step.

7. When the mask is done, we etch the sample using Ar-ion milling, with energies of 1.5-3.5 KeV and currents of $20 - 120\mu A$.

FIG. 3: CRESTEC BABLE 9000 high resolution electron beam lithography system (2 nanometer spot sized beam) at Bar-Ilan institute of Nanotechnology and advanced materials

C. Measurement setup

The magnetoresistance of the superconducting networks was measured in the Quantum Design Physical Property Measurement System (PMMS) shown in figure 4. Sample environment controls include fields up to 9 Tesla and a temperature range of 1.85 - 400 K.

FIG. 4: Quantum Design Physical Property Measurement System (PPMS) installed at the Bar-Ilan Institute of Nanotechnology and Advanced Materials

III. RESULTS

A. Resistance *vs.* Temperature

In this section we describe the measurements results of the superconducting network resistance as a function of temperature, magnetic field and bias-current.

1. R vs. T in different magnetic fields

Figure 5 shows measurements of the network's resistance versus temperature in three different fields: 0, 1480 and 2220 Oe. The resistance increases from zero in the superconducting phase to

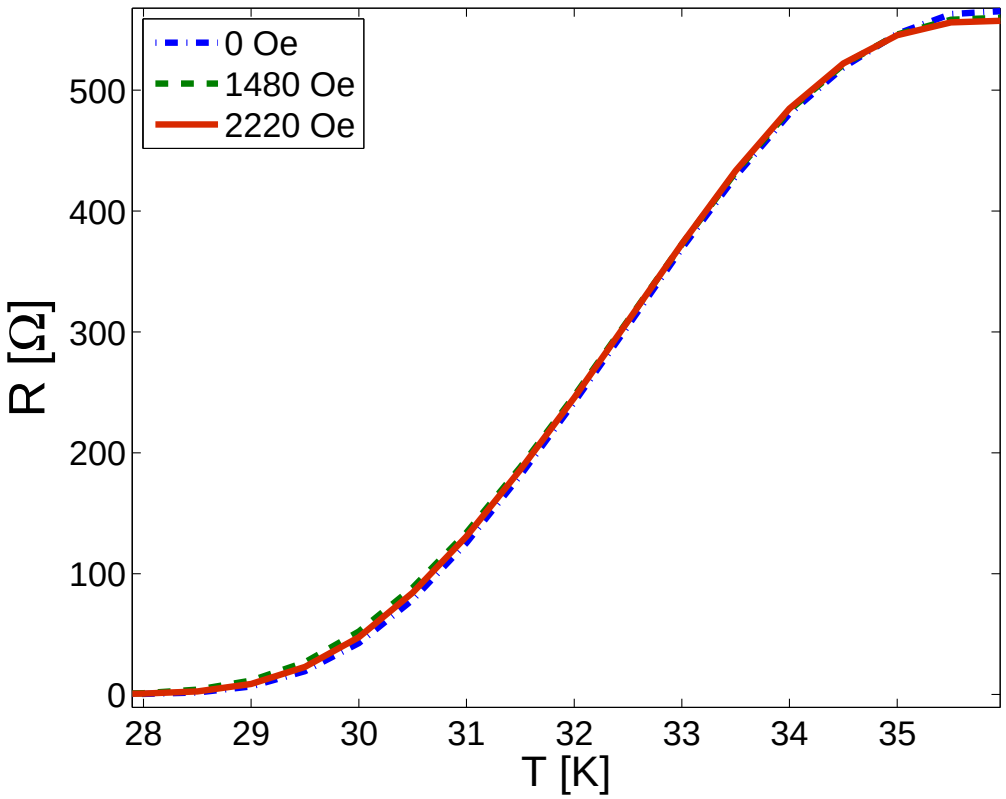

FIG. 5: Resistance *vs.* Temperature measurements in different magnetic fields near the transition temperature. This figure shows the resistance increase with the temperature from zero resistance at the superconducting phase to about 560 Ω in the normal phase.

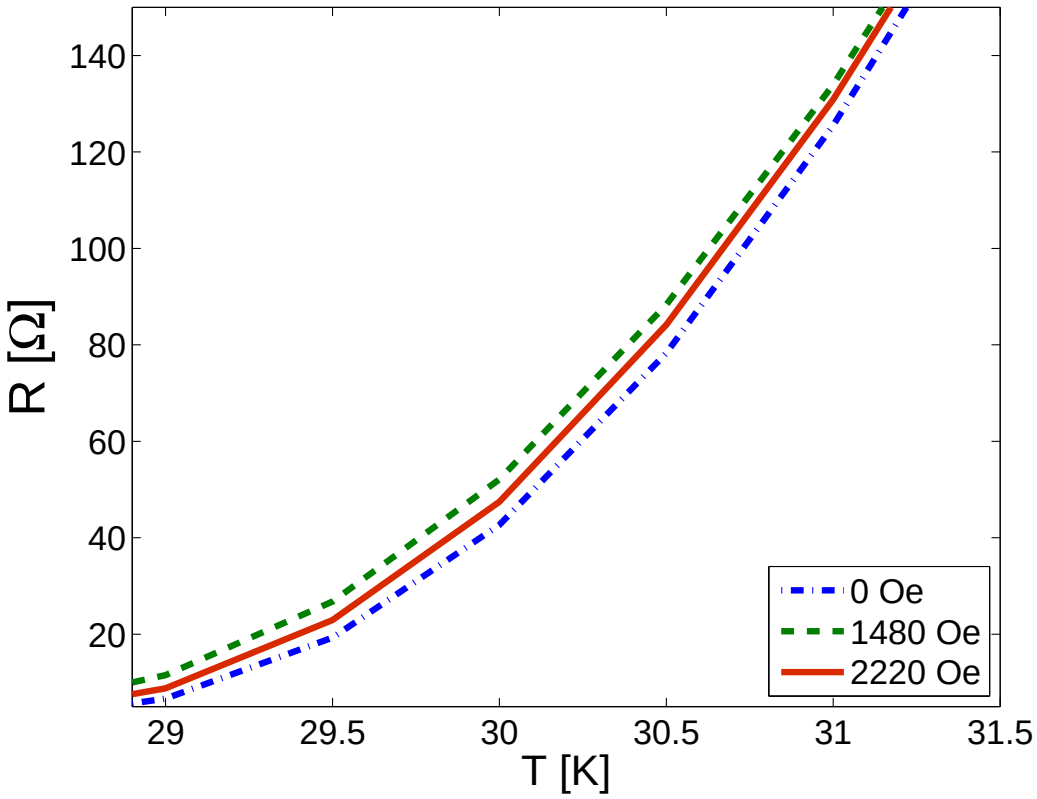

FIG. 6: The resistance *vs.* temperature measurement in different magnetic fields - Zooming in. This figure focuses on the beginning of the transition and shows clearly that the resistance in zero applied field is the lowest among the 3 curves. The curve measured in a field of 1480 Oe has the highest resistance among the 3 curves and when we increase the field to 2220 Oe, we get a curve with lower resistance from the 2220 Oe curve but with higher resistance from the zero applied field curve.

550 Ω in the normal phase with the increase of temperature. In the figure's resolution, the 3 curves corresponding to the different fields overlap. In figure 6 we zoom on the R *vs.* T data in a smaller temperature range, demonstrating a non monotonic behavior of R with the field; the figure shows low resistance curve for zero magnetic field, highest resistance for H = 1480 Oe and mid-range resistance at H = 2220 Oe. This behavior is a part of oscillatory behavior of R vs H which will be described later in section *B* of this chapter.

2. R vs. T in different bias currents

Figure 7 shows temperature dependence of the resistance measured with different bias currents. Apparently, as the bias currents increases, R increases and the transition broadens. These results are consistent with previous measurements in thin films of $YBa_2Cu_3O_{7-\delta}$ [21].

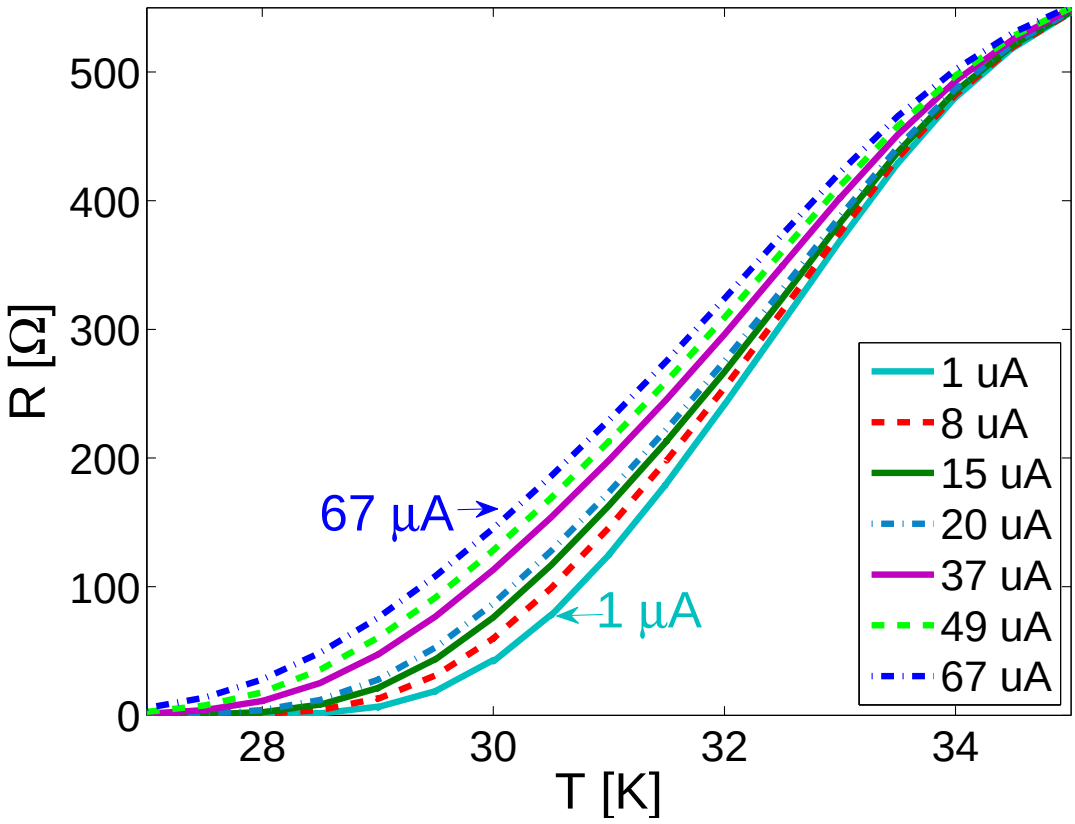

FIG. 7: Resistance *vs.* Temperature in different bias currents. This figure measured near T_c shows the superconducting transition in different bias currents. As we increase the bias current, the transition broadens to a higher temperature range.

B. Magnetoresistance

In this section we present magnetoresistance measurements at different temperatures and bias currents.

1. *R vs. H in different temperatures*

Figure 8 shows R *vs*. H data measured at I = 1.35 μA in several temperatures near T_c. The results show oscillations of the resistance with the magnetic field. In the discussion chapter we will

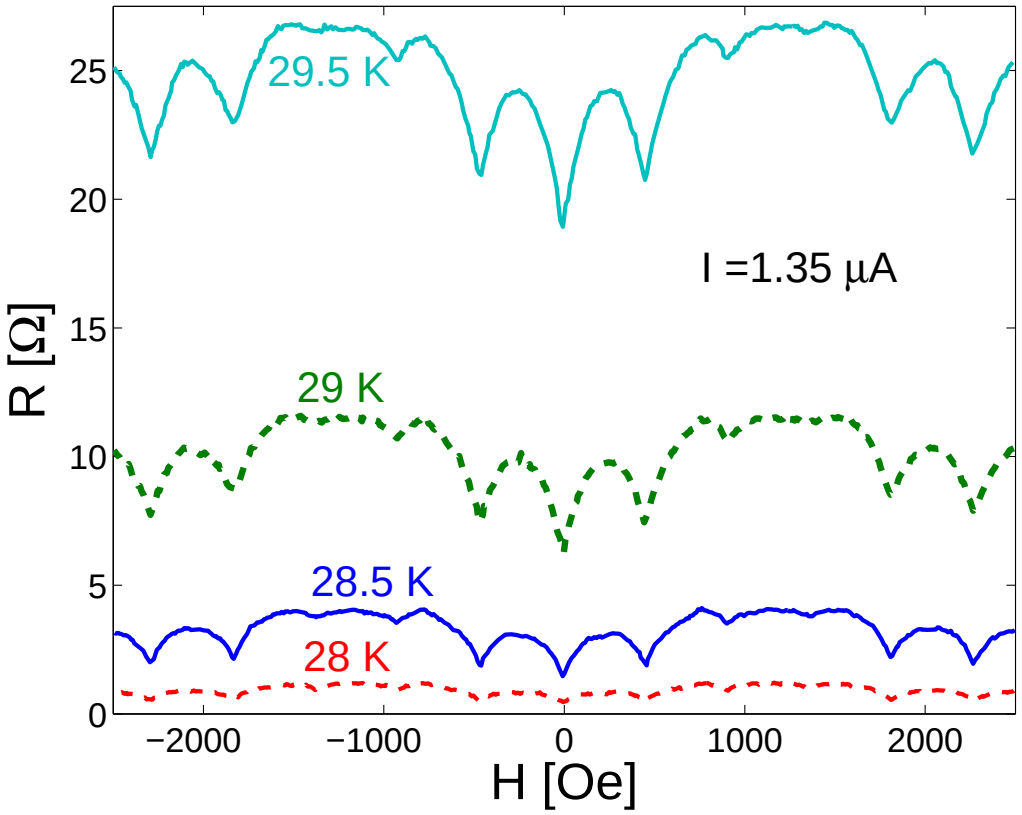

FIG. 8: Magnetoresistance measurements at different temperatures and constant bias-current of 1.35 μA. This figure shows an oscillatory dependence of the resistance in the magnetic field. These magnetoresistance oscillations gain amplitude as the temperature increases in this range of temperatures. The resistance in zero applied field increases as well as we get closer to T_c, as shown in figure 9.

compare these results to the Little-Parks model and to the fluxoid dynamics model for clarifying which mechanism is responsible for the observed oscillations.

The oscillations frequencies are correlated to the sizes of the loops: The magnetic field periodicity corresponding to the area (a^2) of the loop can be calculated by: $H_P = \Phi_0/a^2$, where $\Phi_0 = hc/2e$ is the flux quantum and a is the side of the loop. The small loops magnetic field periodicity is about 2281 *Oe* which corresponds to a loop side length of approximately 94 *nm*. The large loops periodicity is 454 *Oe* and corresponds to 210 *nm*.

2. R vs. H in different bias currents

Figure 9 shows an oscillatory behavior of the resistance with the magnetic field for different bias currents measured at a constant temperature of 28.5 K. To show the oscillations in different bias-currents side by side, we subtracted R_0, the resistance in zero magnetic field $(R(H=0))$, from each R *vs.* H curve. This allows a qualitative comparison between the oscillations measured in different currents. One may see that the amplitude of the oscillations in this particular temperature is a non-monotonic function of the bias current; increasing the bias current from 1.3 μA to 11 μA increases the amplitude of the oscillation significantly. Further increase of the bias current to

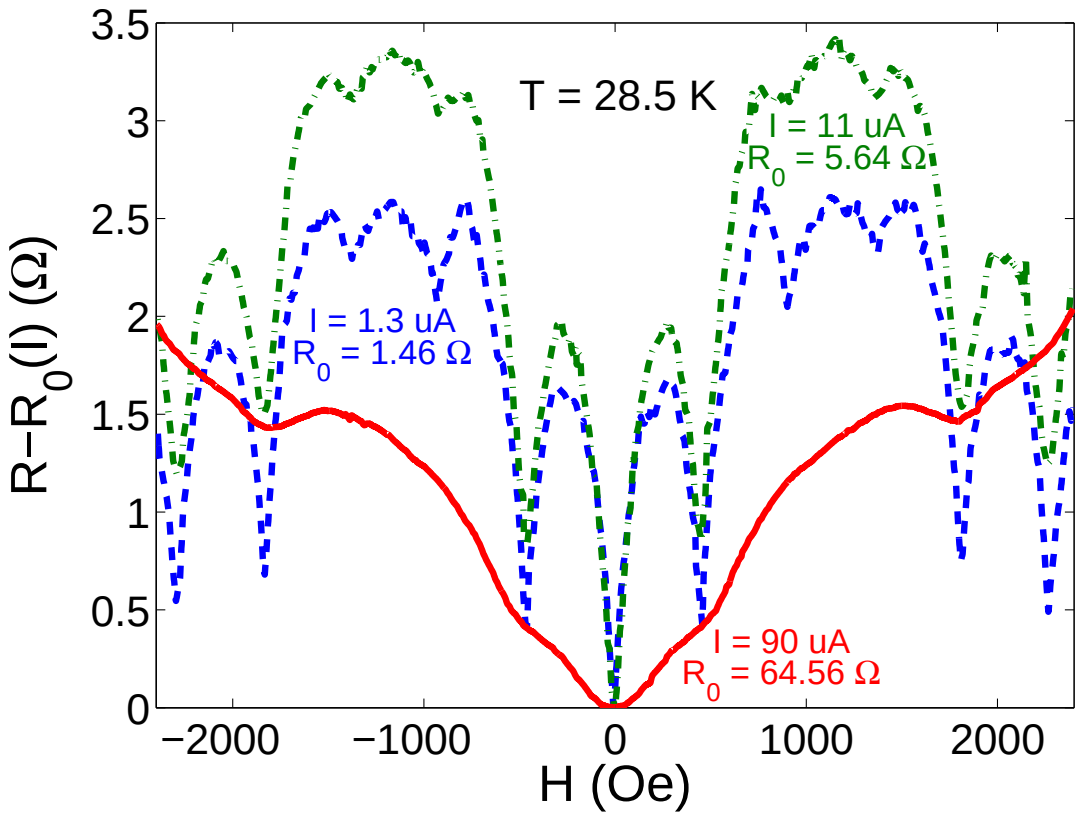

FIG. 9: Magnetoresistance measurement in a fixed temperature of 28.5 K but in different bias-currents. The resistance of R(H=0) is reduced from these curves to view side by side the difference between them. The figure shows a non-monotonic dependence of the magnetoresistance oscillations on the bias current. This specific temperature was chosen to show that in high currents (I = 90 uA in the figure), the oscillations are small but in the mid-range current (I = 11 uA) the amplitude is larger than in the lowest current (I = 1.3 uA).

90 μA decreases the oscillations amplitude dramatically. Such measurements were preformed for different currents in the range of 0.5 - 800 μA. On the basis of these measurements we extracted the dependence of the oscillations amplitude on the bias current as described in the next section.

C. Amplitude of the oscillations

The oscillations' amplitude is measured from the lowest resistance, in zero magnetic field, to the first peak of the oscillations, as illustrated in figure 10. This figure schematically describes how we measure the oscillations amplitude of the large loops (ΔR_L) and of the small loops (ΔR_S). Since the amplitudes exhibit the same behavior, we focus in this dissertation on the small loops amplitude (ΔR_S) only and relate to it as ΔR.

The dependence of the amplitude on the temperature and on the bias current is described in the next paragraphes.

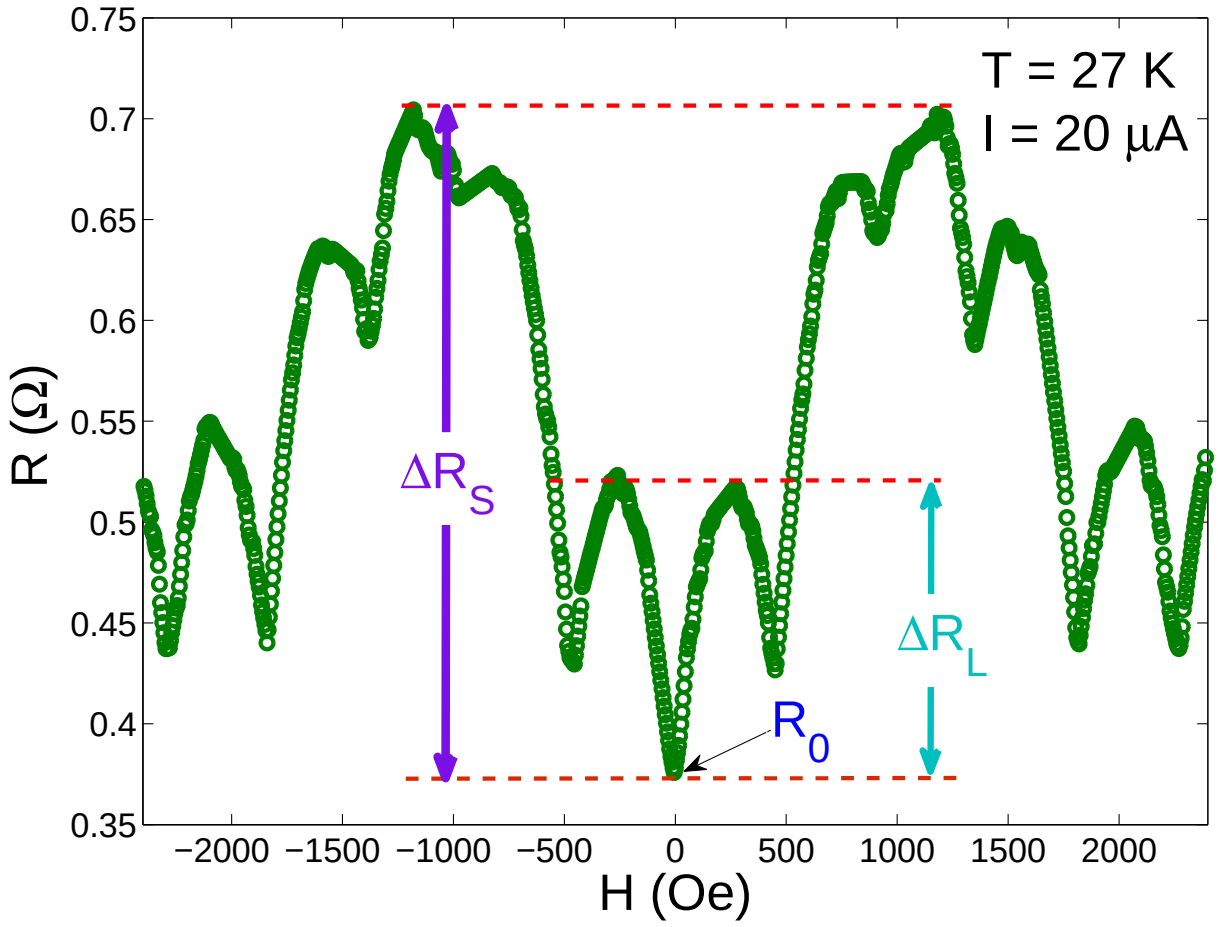

FIG. 10: R *vs.* H in $27K$ and with $20\mu A$ applied. Where $R_0 = R(H = 0)$. ΔR_S is the oscillations' amplitude of the small loops and ΔR_L is the oscillations' amplitude of the large loops.

1. Temperature dependence

Figure 11 describes the behavior of ΔR as a function of temperature for different bias currents between 1.35 μA and 8.16 μA. Apparently, ΔR exhibits a non-monotonic dependence on temperature for all measured currents in this range, with a peak that slightly moves toward a lower temperature as the bias current increases. Also, the amplitude of the effect is clearly bias current dependent, it decreases as the bias current increases.

This behavior can be explained as follows: At low temperatures we do not expect to see (oscillations in) the resistance due to perfect superconductivity. On the other hand, at high temperatures

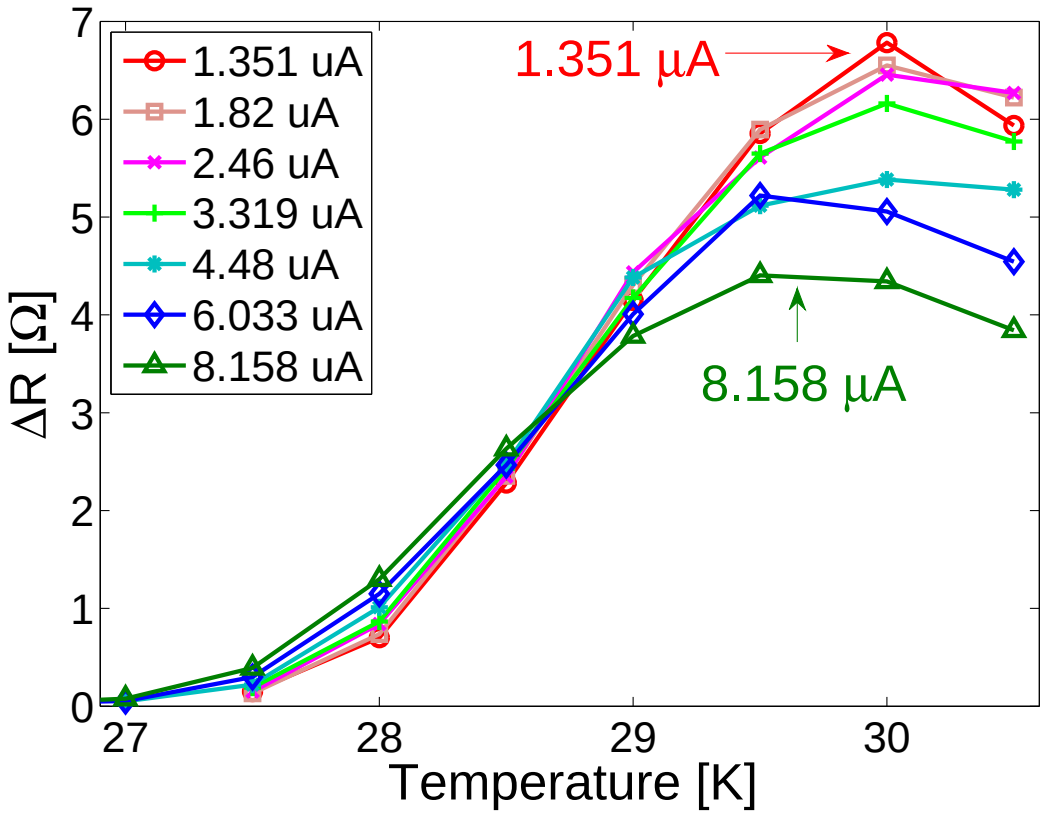

FIG. 11: Amplitude ΔR *vs*. *Temperature* in different bias-currents. This figure show that the oscillations amplitude increase with the temperature until it reaches a peak and then decreases near T_c. The peak for the larger bias currents is lower in amplitude and is at lower temperature than that measured at low currents. Apparently, at temperatures lower than about 28.7 K, the oscillations amplitude of the higher currents is larger.

we expect the oscillations amplitude to decrease as we approach T_c. Therefore, we expect (and observe) a non-monotonic behavior of the oscillations amplitude with temperature. In the discussion chapter we elaborate on this behavior in more details in the framework of both the Little Pakrs and the fluxoid dynamic model.

2. Bias-current dependence

Figure 12 describes the oscillations amplitude as function of the bias current in different temperatures. For clarity, we focus in figure 13 on 5 temperature curves. In these figures we can see:

1. A monotonic increase of ΔR with I at low temperatures.
2. A non monotonic behavior of ΔR with I at mid-range temperatures.
3. A monotonic decrease of ΔR with I near T_c.

Figures 12 and 13 show that the bias current in which the peak of the amplitude occurs decreases as the temperature increases. Therefore, we may assume that the mid-range temperatures

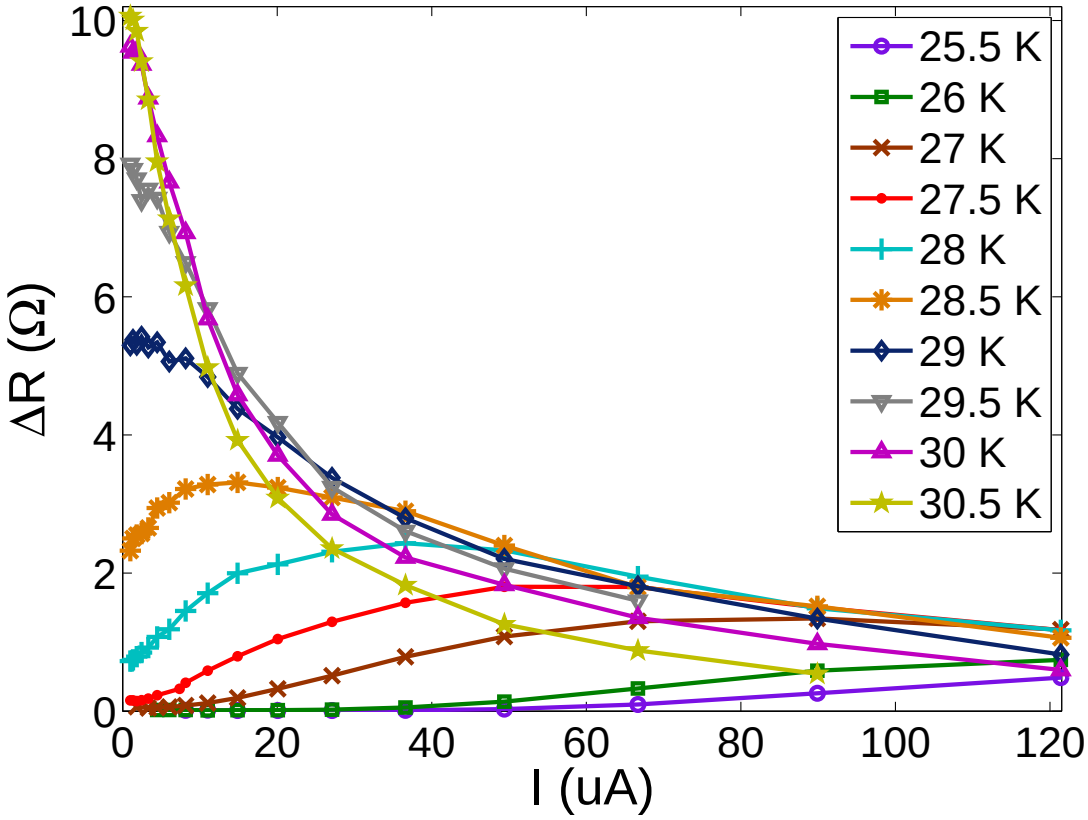

FIG. 12: Amplitude ΔR *vs. bias current* in different temperatures. This figure shows that at low temperatures ΔR increases with the bias currents. In mid-range temperature, ΔR has a non-monotonic behavior and it reaches a peak and at high temperatures, ΔR decreases with the bias current.

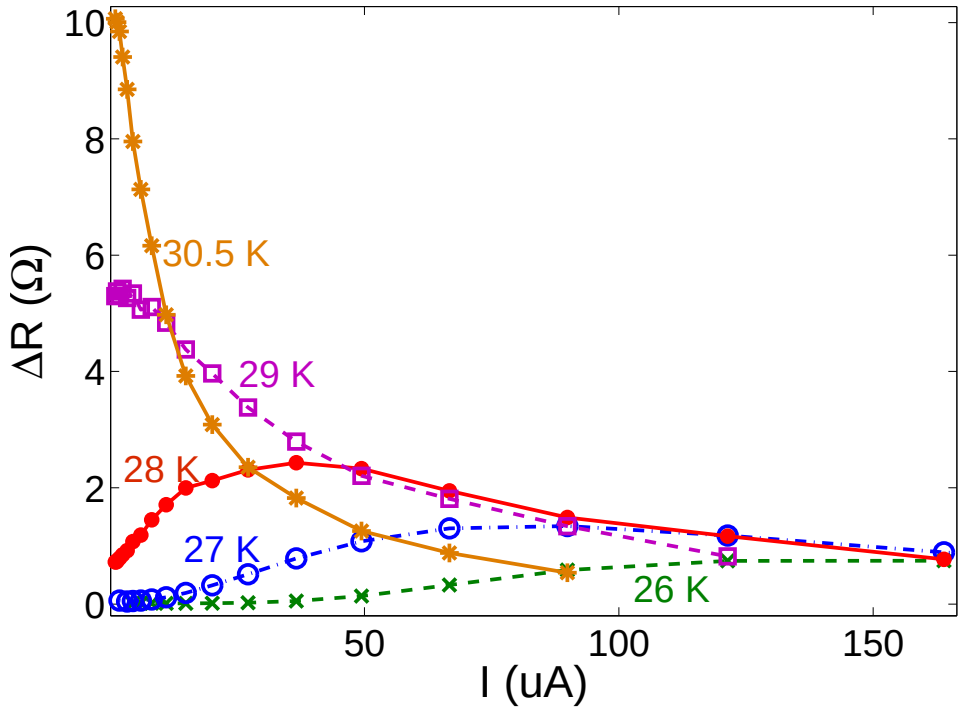

FIG. 13: Amplitude ΔR *vs*. *bias current* in different temperatures. This figure focuses on only 5 temperature curves that shows the 3 behaviors described on the last figure.

represent the general behavior of the system. In other words, a peak is expected also at low temperatures but it is pushed to high bias currents that are beyond our experimental capability. Similarly, close to T_c we do not have the bias-current resolution to notice the increase of the low bias currents amplitude.

D. I-V characteristics

Figure 14 exhibits the measured I-V curves in log-log scale at zero magnetic field for temperatures between 7 and 33 K. At low temperatures, the I-V curves experience a linear behavior at low bias currents and exponential behavior in high bias currents with crossover at a current $I_{c.o.}$. At high temperatures the I-V curves are almost complectly linear. From the steep slope we can find the power of the exponential behavior and based on the theoretical predictions of Kogan [18], derive the magnetic penetration depth λ, as discussed in the next chapter.

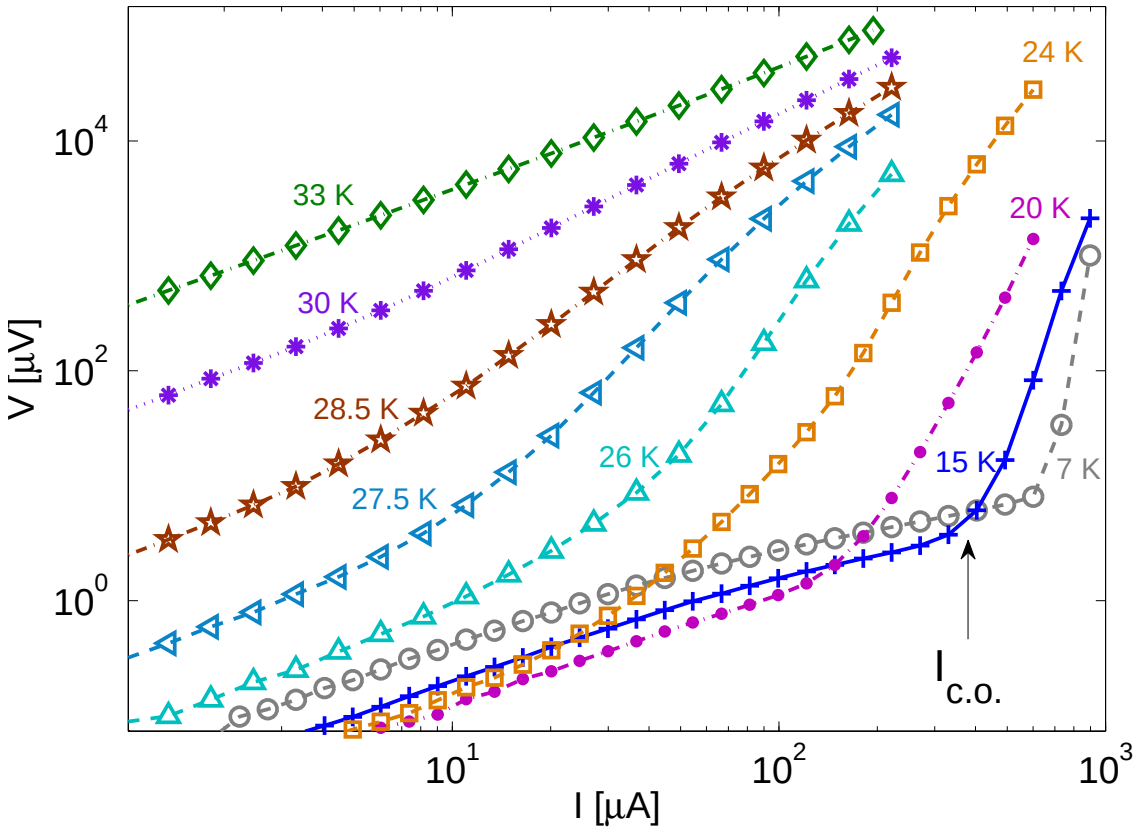

FIG. 14: A log-log plot of Voltage *vs*. Current measurements in different temperatures. $I_{c.o.}$ is an example of the crossover curent from linear to power-law behavior.

IV. DISCUSSION

A. Comparing the results to the Little-Parks model

The Little-Parks model ascribes the magnetoresistance oscillations to periodic changes in the transition temperature with the magnetic field.

According to this model, T_c moves back and forth as the magnetic field is increased, due to periodic changes in the kinetic energy of the system as function of magnetic field.

As mentioned in the introduction, the Little-Parks model predicts that the amplitude, ΔT_c, of the changes in T_c is given by equation 5 and the amplitude of the magnetoresistance oscillations, ΔR can be approximated by equation 6.

1. Temperature dependence

Figure 15 shows the Little-Parks model prediction for $\Delta R_{L.P.}$ *vs*. temperature (circles), derived by equation 6 and using the experimental dR/dT of figure 7, together with the experimental results of ΔR *vs*. T (squares), for two different bias currents (1.35 uA and 49.4 uA).

The figure shows that both the experimental ΔR and the predicted $\Delta R_{L.P.}$ increases with temperature until a maximum point (a peak) obtained at a certain temperature and then the amplitude decreases as the temperature continues to increase towards T_c.

One can see, however, that although the Little-Parks model predicts the qualitative behavior of ΔR *vs*. T, it differs largely from the experimental results in both the maximum value of ΔR and the temperature at which this value is obtained. The maximum value of the experimentally measured ΔR is larger by more than an order of magnitude from that expected from the Little-Parks model. The temperature at which the peak value of ΔR is obtained is shifted down in the experiment be several degrees. In addition, the effect of increasing the bias current is much more pronounced in the experiment. A more detailed comparison of the experimental results and the Little-Parks prediction concerning the effect of the bias current is given in the next subsection.

2. Bias current dependence

The origin of the bias current dependence of ΔR in the Little-Parks model is the fact that $\frac{dR}{dT}$ is not only temperature dependent but also bias current dependent. Figure 16 shows the expected amplitude from the Little-Parks effect as function of the bias current at temperatures between 27 and 32 K. The current dependence of $\frac{dR}{dT}$ was derived from figure 7. Figure 16 shows that the amplitude increases with the bias current for temperatures between 27 to 29.5 K. The 30 K curve exhibits a saturation as the bias current increases above $20\mu A$, while the 32 K curve shows a monotonic decrease for all the measured bias currents. For a comparison we show in figure 17 the experimentally measured amplitude of the oscillations as function of the bias current.

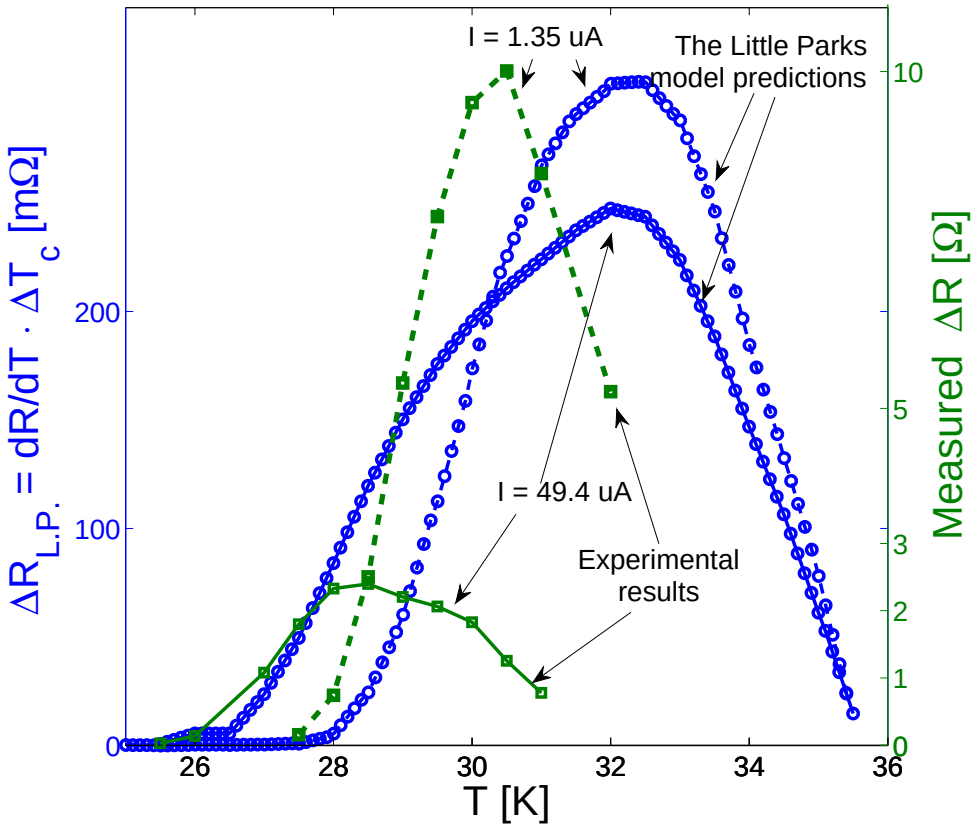

FIG. 15: Comparison between the experimentally measured amplitude ΔR *vs*. Temperaure (squares) and the prediction of the Little-Parks model (circles) in 2 different bias currents. The Little-Parks model curves correspond to the left Y axis which is measured in $m\Omega$ and the experimental results curves correspond to the right Y axis measured in Ω

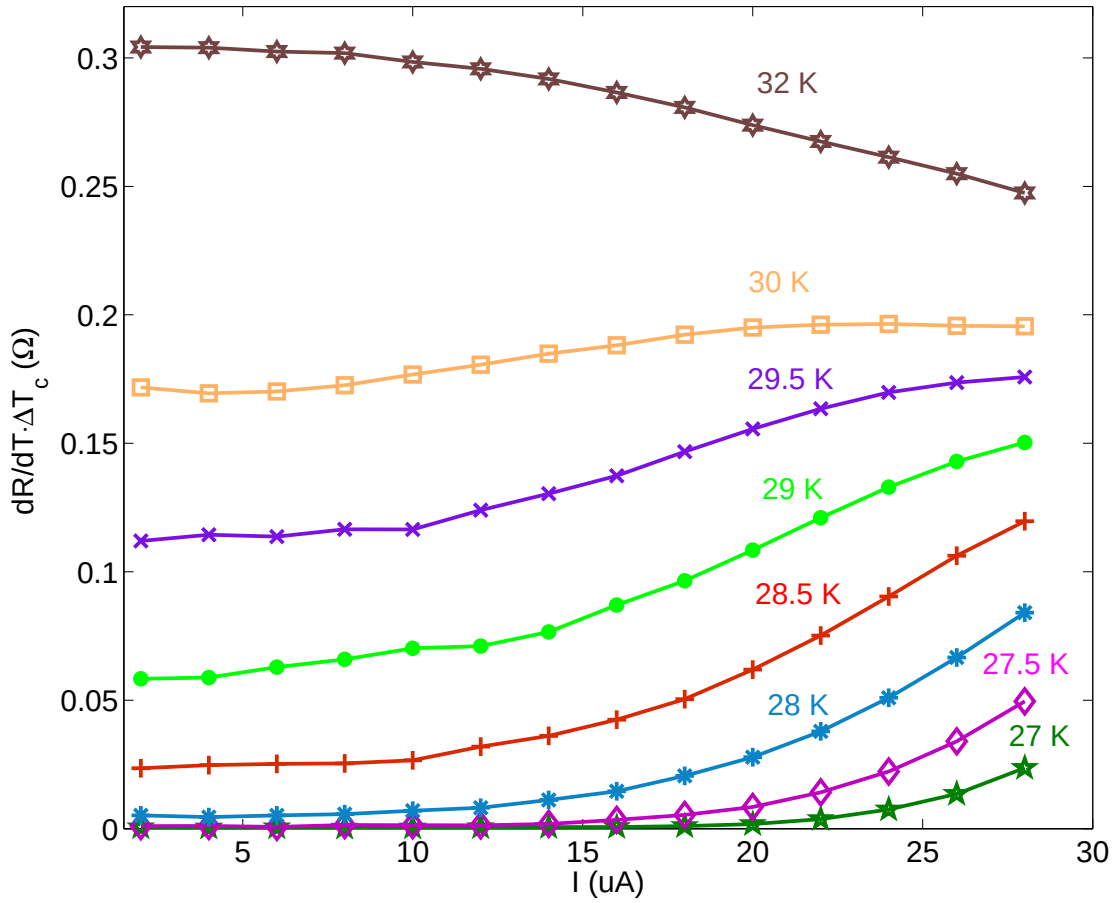

FIG. 16: The Little-Parks model prediction of the oscillations amplitude dependence on the bias-current, measured in different temperatures.

As opposed to the Little-Parks prediction, the experimental results of figure 17 show that ΔR decreases with the bias current already at 29 K and continuous to decrease sharply with the bias current as the temperature is increased. Moreover, the measured peak value of ΔR at 30 K is approximately 5 Ω while the Little-Parks model predictions is about 0.17 Ω. We conclude that the Little-Parks model cannot explain our data.

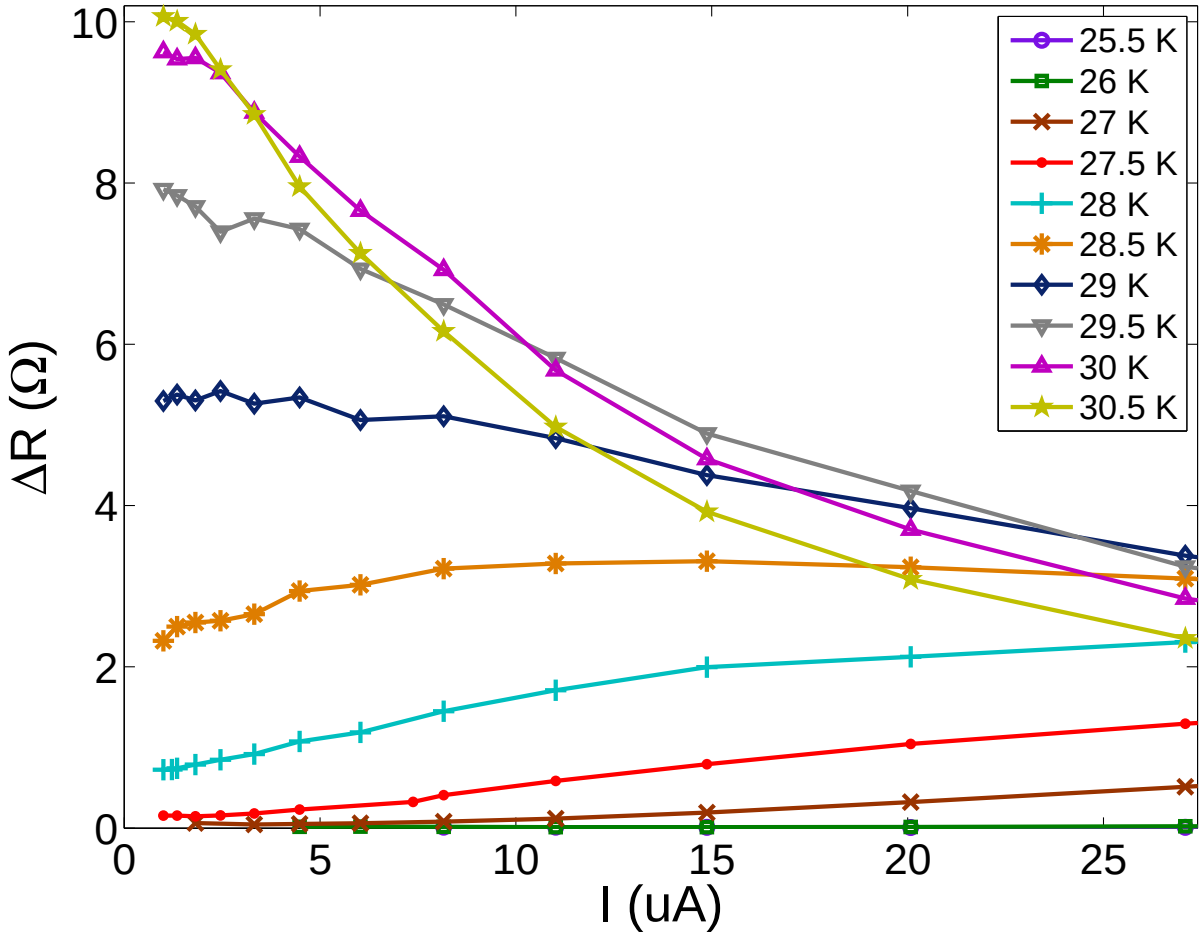

FIG. 17: Oscillations amplitude dependence on the bias-current, measured at different temperatures.

B. Comparing the results to the fluxoid dynamic model

The fluxoid dynamic model suggested by Sochnikov *et al*. for the magnetoresistance oscillations was described in section *C* of the introduction. However, this model did not take into account the bias current effect on the oscillations amplitude. In this work, we extended this model using Kogan's theory [18] for the bias current dependence of the energy needed for creating of a vortex in wire. Kogan's theory was developed to explain I-V curves measured in thin superconducting wires. To test the applicability of this theory to our networks, we first compared our I-V measurements (figure 14) in those networks with the theory.

1. I-V curves and macroscopic properties

As is apparent from figure 14, the I-V curves exhibit two regions: a linear region at low bias-currents and a power law region at high bias currents. We mark the crossover bias-current, $I_{c.o.}$, in which the behavior changes from linear to power-law and plot it in figure 18 as a function of temperature. Apparently, the crossover current is decreasing as the temperature increases.

The power law behavior fits the prediction of Kogan theory. According to this theory, the power, m, of the I-V curve in the power-law region is associated with the London penetration

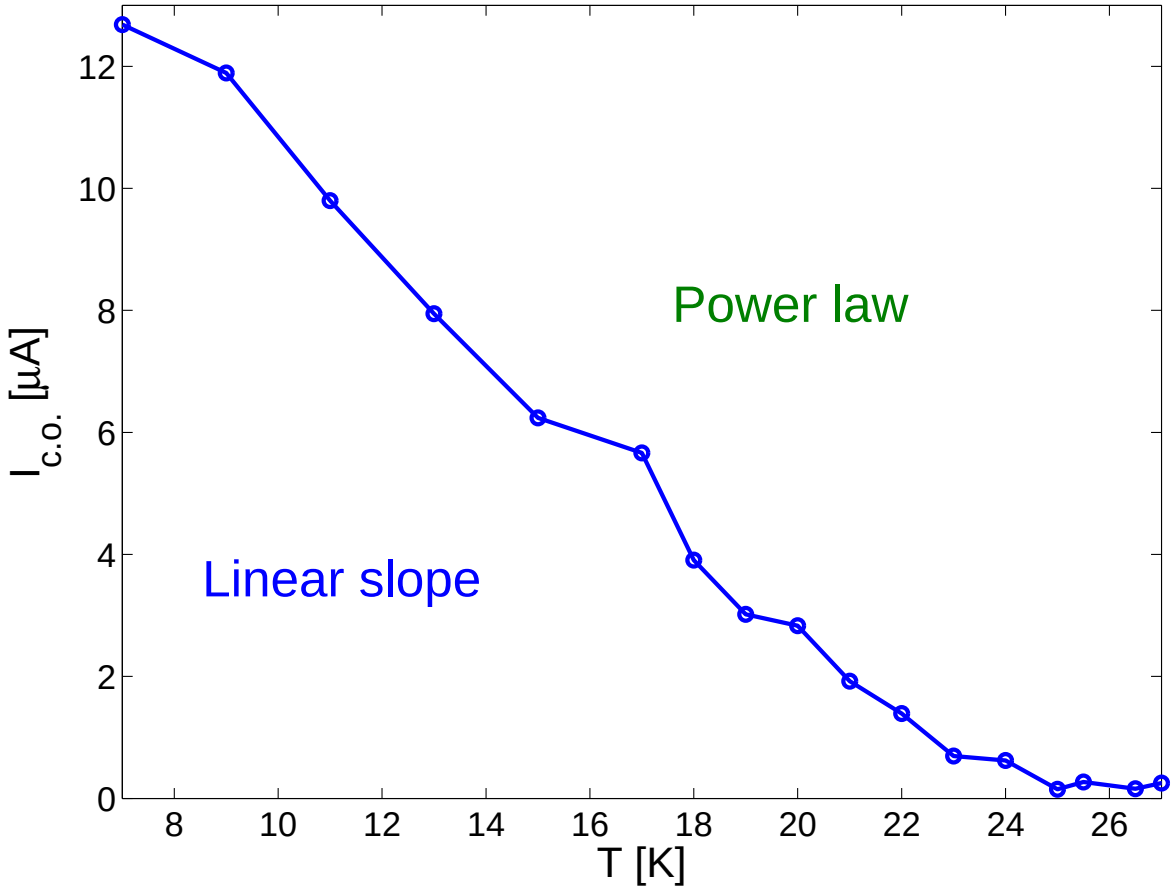

FIG. 18: Temperature dependence of the crossover current, $I_{c.o.}$, separating between the linear and the exponential regions. This figure shows $I_{c.o.}$ decreases when increasing the temperature. The solid line connects the points derived from the experimental data.

depth λ [18]:

$$\lambda = \frac{\phi_0}{4\pi}\sqrt{\frac{ln(b/a)d}{(m-1)k_BT}}, \tag{7}$$

where ϕ_0 is the flux quantum, d is the thickness of the film, b is the outer side of the loop and a is the inner side, m is the power of the I-V curve in the power-law region, k_B is Boltzmann's constant and T is the temperature in Kelvin.

In figure 19 we plot λ values (circles) extracted from the data of figure 14 at the measured temperatures. We compare it with the theoretical prediction for the penetration depth dependence on temperature (solid curve) [22]:

$$\lambda = \frac{\lambda_0}{\sqrt{1-(T/T_c)^2}} \tag{8}$$

where λ_0 is the penetration depth in absolute zero. Our two fitting parameters are T_c and λ_0. Fitting equation 8 to the extracted data, we get the fitting parameters $T_c = 33K$ and λ_0 =900 nm,

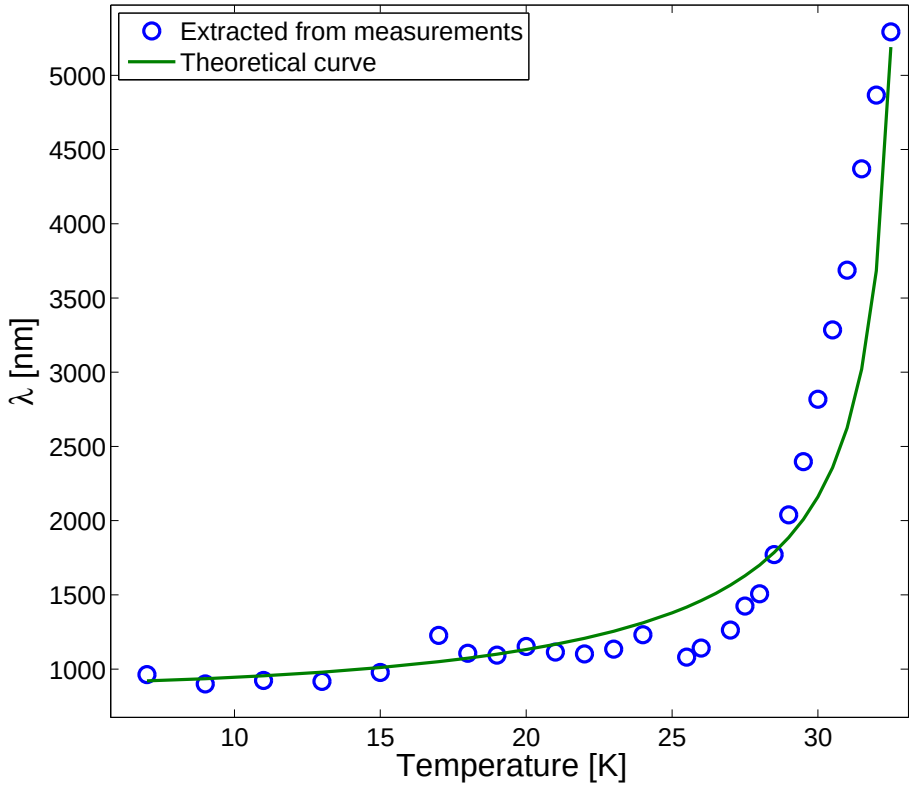

FIG. 19: λ *vs. Temperature* derived from the I-V curves. This figure shows the penetration depth is increasing with the temperature and diverges near T_c. The solid line is a fit to equation 8.

using d = 24 *nm* and a = 95 *nm* , b = 120 *nm*. This value of λ_0 is comparable with published results. (For example, Sochnikov *et al*. [10] report on λ_0 = 750 nm and about the same T_c in similar $La_{1.84}Sr_{0.16}CuO_4$ but with different patterning). This result shows that Kogan's model can be used in our case for currents larger than I_0.

2. Current-dependent energy barrier

The key parameter in the fluxoid dynamic model is the barrier energy ΔE, that is the energy needed to insert a vortex inside the superconducting wire and drive it across the wire width. The vortex interacts with a fluxoid current in the superconducting loop and the energy associated with this interaction oscillates with the magnetic field.

The barrier energy, ΔE is approximated by [10, 11, 17]:

$$\Delta E \approx E_v + \left(\varepsilon_0 \left(n - \frac{\Phi}{\Phi_0}\right)\right)^2 - (\mu H \tanh\left(\frac{\mu H}{k_B T}\right) \tag{9}$$

where E_v is the energy required to create a vortex and drive it across the wire. The second term on the right hand side of equation 9 describes the interaction of the vortex with the fluxoid current. The third term describes the interaction of the vortex with the external magnetic field. This last term is responsible for the background of the magnetoresistance measurement. This term can be approximated by $\frac{(\mu H)^2}{k_B T}$ when $\mu H \ll k_B T$. Since we deal only with low magnetic fields where the background is small, this term may be neglected.

In this work we adopt Kogan's expression for the the energy barrier E_v, taking into account its bias current dependence [18]:

$$E_v = \varepsilon_0 \left(ln \left(\frac{2W}{\pi\xi \sqrt{1 + I^2/I_0^2}} \right) - \frac{I}{I_0} \tan^{-1}\left(\frac{I_0}{I}\right) \right), \tag{10}$$

where

$$\varepsilon_0 = ln(b/a) \frac{\Phi_0^2}{8\pi^2 \Lambda} \tag{11}$$

and

$$I_0 = \frac{c\Phi_0}{8\pi\Lambda} \tag{12}$$

W is the width of the loop's wire, ξ is the coherence length of the superconductor, a and b are the inner and outer sides of the loop respectively, $\Lambda = 2\lambda^2/d$ is the Pearl length [23], and d is the thickness of the superconductor, c is the speed of light in vacuum. When the bias current $I \gg I_0$ the expression can be approximated:

$$E_v(I \gg I_0) \approx \varepsilon_0 \ln\left(\frac{2WI_0}{e\pi\xi I}\right) = \varepsilon_0 \ln\left(\frac{I_d^{Kogan}}{I}\right), \tag{13}$$

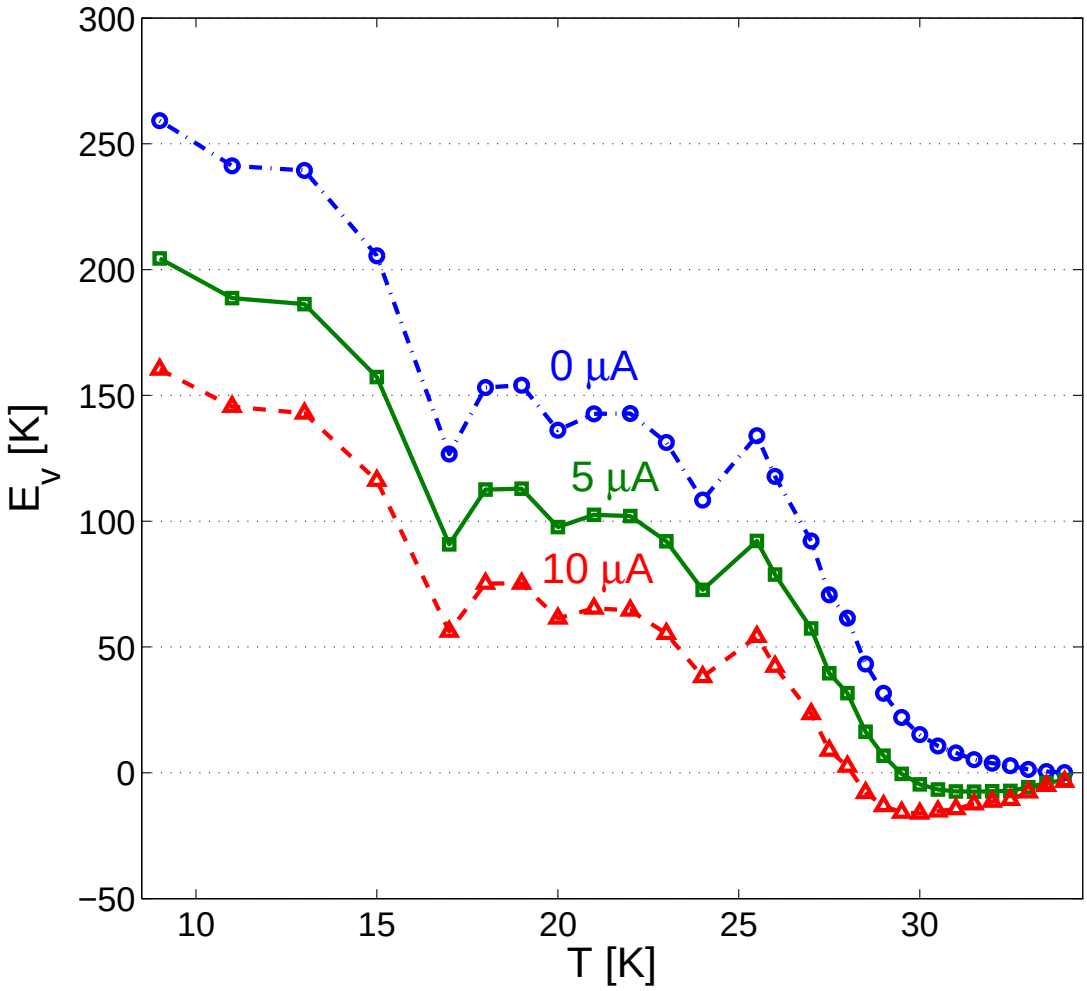

FIG. 20: *E_v vs. Temperature* from the extracted Λ. This figures shows the barrier energy, E_v, decreases with the temperature and with the bias current. In currents higher than 0 μA, notice that E_v crosses the X axis before it reaches to T_c in a point of critical current where we expect the loop to become normal. The lines in the figure connect the points derived from the data.

where

$$I_d^{Kogan} = \frac{c\phi_0 W d}{8e\pi^2\lambda^2\xi} = I_{depairing}/e \tag{14}$$

This approximated expression for E_v (equation 13) is compatible with Zeldov's logarithmic barrier model [24, 25] asserting that $E \propto \ln(J_c/J)$. Thus, we expect the barrier energy, E_v to decreases with temperature and current and goes to zero when $T \to T_c$ or when $J \to J_c$.

In order to estimate the range of validity of the logarithmic approximation given in equation

13, we plot in figure 21 the energy barrier with and without the high current approximation at 22 K. One can see that at this temperature, the approximation is valid for currents greater than $I_0 \approx 6$ μA at temperature of 22 K. The same procedure was carried out to estimate I_0 in the temperature range 5 to 36 K and the results are shown in figure 22.

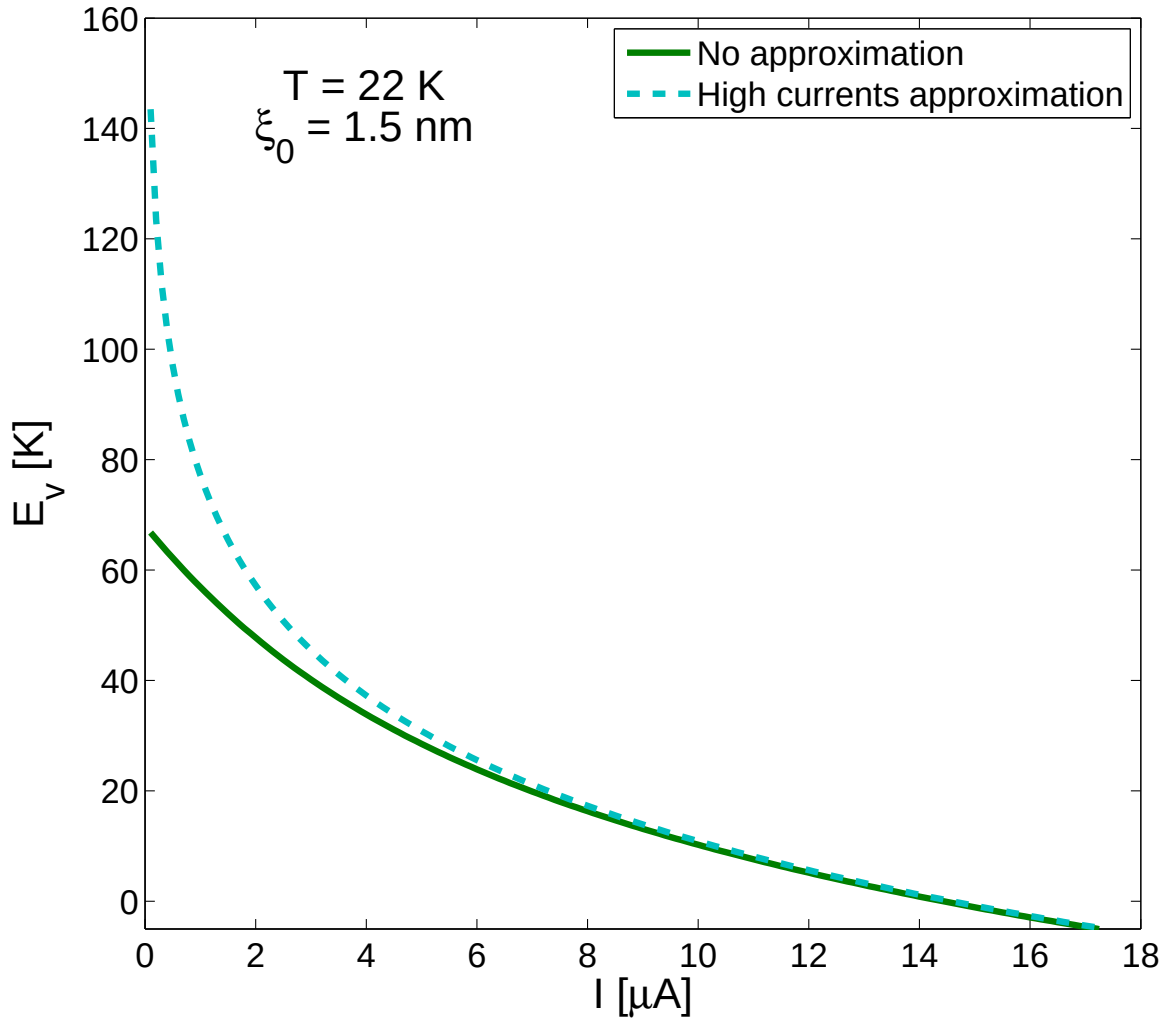

FIG. 21: The energy barrier *vs*. bias-current. The solid line is a plot of equation 10 and the broken line represents the approximation in equation 13.

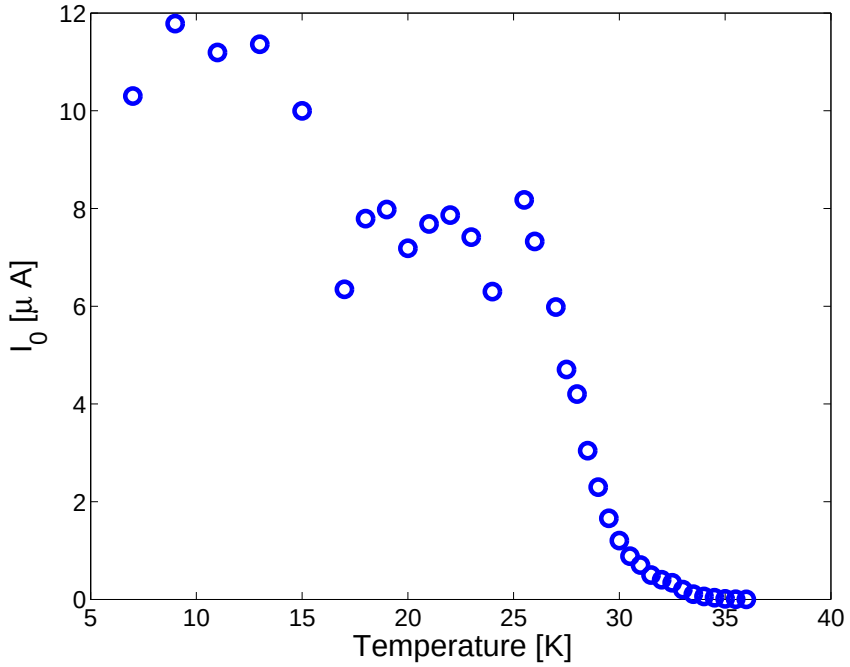

FIG. 22: I_0, the current above which in which the approximation to E_v is valid, as function of temperature. This I_0 *vs*. T plot shows a drop to zero of I_0 as we get close to T_c.

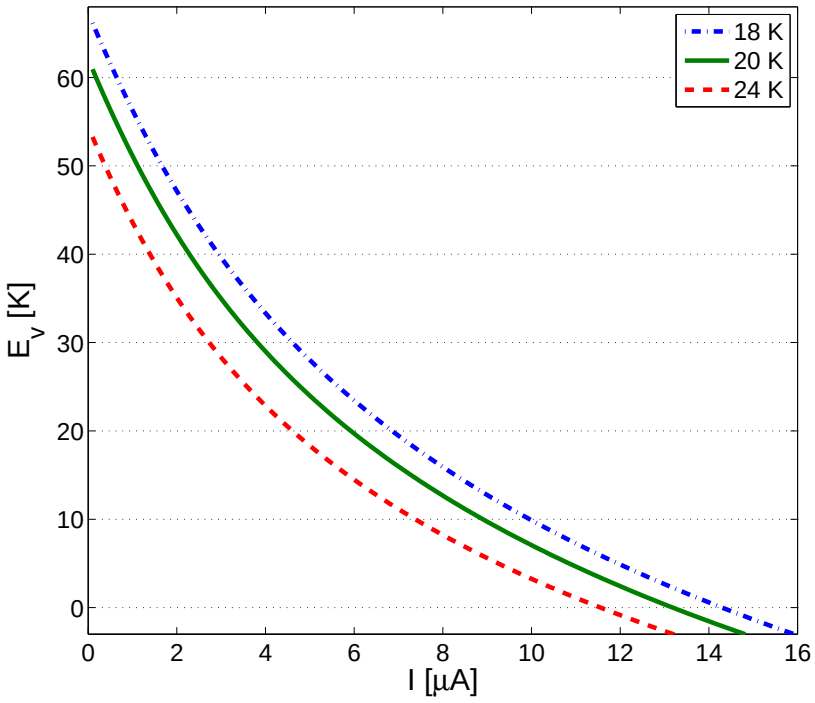

FIG. 23: The energy barrier *vs*. bias-current in different temperatures. This plot shows that the barrier energy decreases as the temperature or the bias current increase.

3. Oscillations amplitude

Based on the Ambegaokar-Halperin [26] and Tinkham [27] works connecting ΔE with the resistance, we find:

$$R(I,T,H) \approx R_n \left[\mathfrak{I}_0 \left(\frac{E_v(I,T)}{2k_BT} - \left[\frac{E_0(T)(n-\Phi(H)/\Phi_0)}{k_BT} \right]^2 /2 \right) \right]^{-2} \tag{15}$$

where $\mathfrak{I}_0$ is the modified Bessel function, E_0 equals to ε_0 ,R is the resistance which is an oscillating function of the magnetic field and it depends on the temperature and bias current, and R_n is the resistance of a single loop in the normal state. Yet, Ambegaokar and Halperin derived this equation using low currents approximation, while we use Kogan's approximation for currents higher than I_0. Thus, we expect to obtain a good fit only in narrow range of currents where both approximations are valid.

To calculate the oscillations amplitude, we subtract R at $\Phi = 0$, where the energy is minimal due zero fluxoid currents, from R at $\Phi = \frac{1}{2}\Phi_0$, where the lowest energy level is at maximum obtaining:

$$\frac{\Delta R}{R_n} = \left[\mathfrak{I}_0 \left(\frac{E_v(I,T)}{2k_BT} - \left[\frac{E_0(T)(n-\Phi(H)/\Phi_0)}{k_BT} \right]^2 /2 \right) \right]^{-2} - \left[\mathfrak{I}_0 \left(\frac{E_v(I,T)}{2k_BT} \right) \right]^{-2}. \tag{16}$$

Assuming $E_v \gg \varepsilon_0^2/2k_BT$, equation 16 can be approximated by:

$$\Delta R \approx \frac{dR}{dE}_{H=0} \Delta E = R_n \frac{\mathfrak{I}_1(E_v/2k_BT)}{\mathfrak{I}_0^3(E_v/2k_BT)} \left[\frac{E_0}{2k_BT} \right]^2. \tag{17}$$

The solid curve in figure 24 is a fit of this expression to the experimentally measured amplitude ΔR *vs*. I data (circles). In this fit we used $R_n = 64.7\Omega$ ($R_n^{Single} = R_n^{Network} \times \frac{number-of-parallel-connected-loops}{number-of-series-connected-loops}$), $I_d = 6.5\ \mu A$ and $\lambda = 3.4\ \mu m$.

Apparently, the fit is very good up to 3 μA.

Such fits were attempted for other temperatures between 25.5 and 28 K. The results are shown in figure 25. Although the theoretical curves (solid lines) describe well the functional form of the dependence of ΔR on the bias current, in order to fit the amplitude, we had to introduce a normalization factor R_0 which increases sharply with temperature. We noticed that the behavior

of $R_0^{1/4}$ *vs.* temperature resembles that of λ, as shown in figure 26. This led us to assume that the origin of this discrepancy is in the dependence of E_0 on the bias current which was not taken into account in our analysis. Indeed, one has to add the kinetic energy:

$$E_{kinetic} = \frac{1}{2}\frac{4\pi\lambda^2}{c^2}J^2 \tag{18}$$

in the expression for E_0 obtaining:

$$E_0(T,J) = \varepsilon_0(T)\left(1+\frac{2\pi\lambda^2}{c^2\varepsilon_0(T)}J^2\right). \tag{19}$$

Near T_c, $\varepsilon_0 \to 0$ thus $E_0(T,J) \to \frac{2\pi\lambda^2}{c^2}J^2$. This explains the proportionality between $R_0 \propto \lambda^4$ and the origin of the factor R_0.

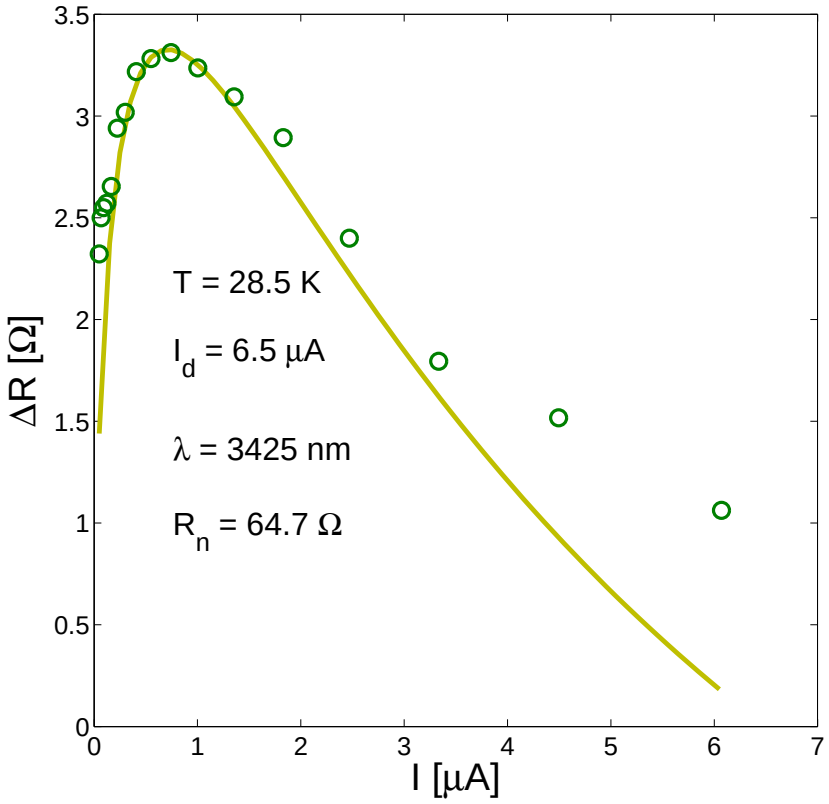

FIG. 24: Amplitude ΔR *vs.* bias current, experimental data (circles) and theoretical fit (solid line). This figure shows a steep slop of ΔR increasing with the bias current, reaching a peak and then decreasing slowly as the bias current increases.

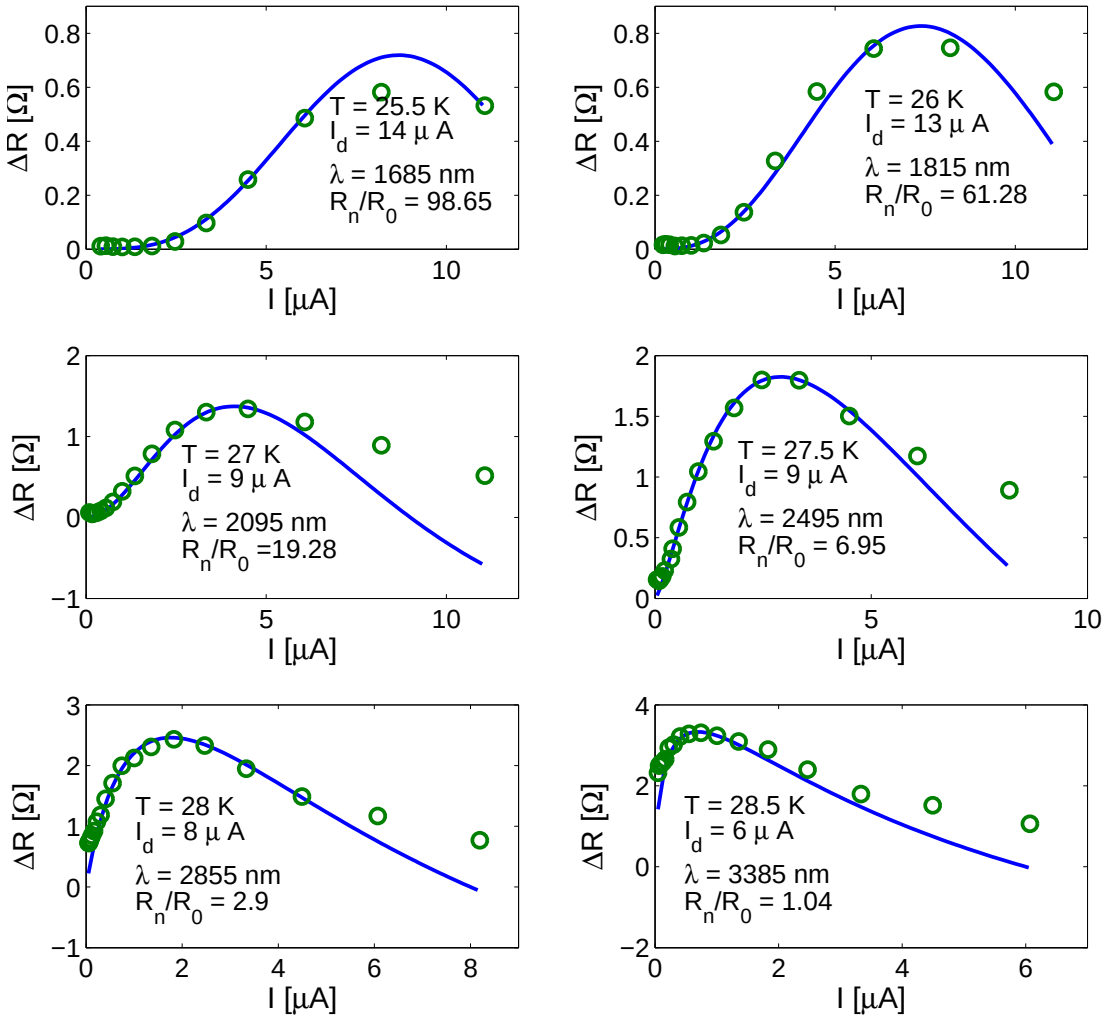

FIG. 25: Amplitude ΔR *vs*. bias current, experimental data and theoretical fits for 6 different temperature. The steep slope in low bias currents observed at 28.5 K (see also figure 24) and down to 27 K, becomes less steep as the temperature drops. Here, R_n/R_0 is the ratio between the real fitting curve amplitude to the one showed in this figure. The solid lines are fits to equation 17 connected by the coefficient R_0

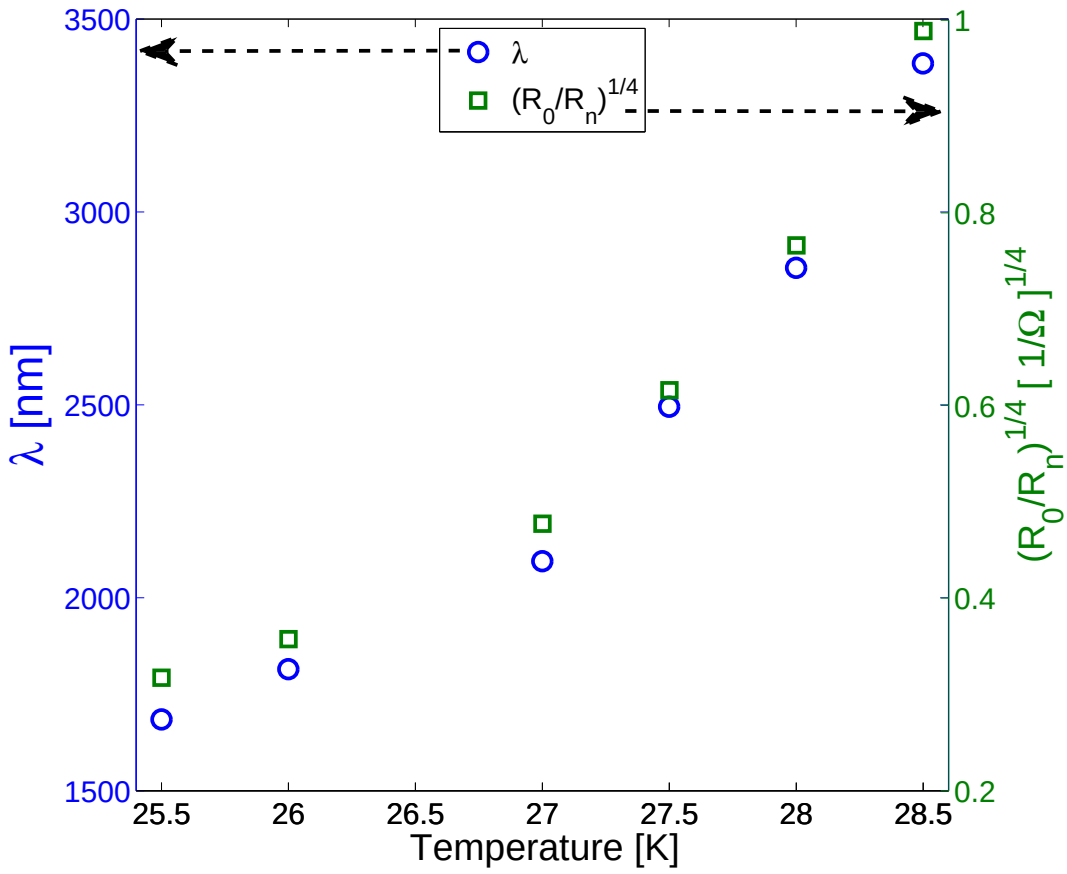

FIG. 26: This figure compares the behavior of λ and $R_0^{1/4}$ as function of temperature. In both, the value increases as the temperature increases in the same way.

V. SUMMARY AND CONCLUSIONS

The results of this work show that the bias current has a dramatic effect on the magnetoresistance oscillations. The amplitude, ΔR, of the oscillations exhibits a non-monotonic dependence on the bias current, with a peak that increases and shifts to lower currents as the temperature approaches the critical temperature, T_c. The peak of ΔR increases by almost an order of magnitude as the temperature increases from 25.5 K to 28.5 K. Attempts to explain these data on the basis of the Little-Parks model were unsuccessful. This model cannot explain neither the oscillations amplitude nor the current dependence of ΔR. In an effort to explain our data in the framework of the fluxoid dynamic model, we extended this model to take into account the current dependence of the energy needed for the creation of a vortex/antivortex in a loop, as well as the interaction energy between the bias current and the vortices. This extended model provides a much better fit to our data. Specifically, it describes well the functional form of the dependence of ΔR on the bias current, as well as the amplitude of the oscillations in the low and mid-range currents in the measured temperature range of 25.5 - 28.5 K. In the higher temperature range, the low current approximation is no longer valid and less satisfactory fits are obtained. In conclusion, the measurements and analysis presented in this work support the fluxoid dynamic model as describing the magnetoresistance oscillations in high-T_c superconductor as first suggested by Sochnikov *et al*.

References

[1] F. LONDON, *Phys. Rev.* **74**, 562 (1948).

[2] W. A. LITTLE and R. D. PARKS, *Phys. Rev. Lett.* **9**, 9 (1962).

[3] R. D. PARKS and W. A. LITTLE, *Phys. Rev.* **133**, A97 (1964).

[4] R. P. GROFF and R. D. PARKS, *Phys. Rev.* **176**, 567 (1968).

[5] Y. AHARONOV and D. BOHM, *Physical Review* **115**, 485 (1959).

[6] M. TINKHAM, *Physical Review* **129**, 2413 (1963).

[7] C. LOBB, *Physica B: Condensed Matter* **152**, 1 (1988).

[8] A. BEHROOZ, M. J. BURNS, D. LEVINE, B. WHITEHEAD, and P. M. CHAIKIN, *Phys. Rev. B* **35**, 8396 (1987).

[9] G. BERDIYOROV, M. MILOŠEVIĆ, M. LATIMER, Z. XIAO, W. KWOK, and F. PEETERS, *Physical Review Letters* **109**, 057004 (2012).

[10] I. SOCHNIKOV, A. SHAULOV, Y. YESHURUN, G. LOGVENOV, and I. BOŽOVIĆ, *Nature Nanotechnology* **5**, 516 (2010).

[11] I. SOCHNIKOV, A. SHAULOV, Y. YESHURUN, G. LOGVENOV, and I. BOŽOVIĆ, *Physical Review B* **82**, 094513 (2010).

[12] I. SOCHNIKOV, I. BOŽOVIĆ, A. SHAULOV, and Y. YESHURUN, *Physical Review B* **84**, 094530 (2011).

[13] I. SOCHNIKOV, Y. SHOKEF, A. SHAULOV, and Y. YESHURUN, *Physical Review B* **84**, 024513 (2011).

[14] I. SOCHNIKOV, Y. SHOKEF, A. SHAULOV, and Y. YESHURUN, **400**, 022110 (2012).

[15] F. CARILLO, G. PAPARI, D. STORNAIUOLO, D. BORN, D. MONTEMURRO, P. PINGUE, F. BELTRAM, and F. TAFURI, *Phys. Rev. B* **81**, 054505 (2010).

[16] P. L. GAMMEL, P. A. POLAKOS, C. E. RICE, L. R. HARRIOTT, and D. J. BISHOP, *Phys. Rev. B* **41**, 2593 (1990).

[17] J. KIRTLEY, C. TSUEI, V. KOGAN, J. CLEM, H. RAFFY, and Z. LI, *Physical Review B* **68**, 214505 (2003).

[18] F. TAFURI, J. KIRTLEY, D. BORN, D. STORNAIUOLO, P. MEDAGLIA, P. ORGIANI, G. BALESTRINO, and V. KOGAN, *EPL (Europhysics Letters)* **73**, 948 (2006).

[19] I. SOCHNIKOV, *Fluxoid Quantization Effects in Superconducting LaSrCuO*, dissertation, Bar-Ilan University, 2011.

[20] A. HOOLE, M. WELLAND, and A. BROERS, *Semiconductor science and technology* **12**, 1166 (1997).

[21] W. K. KWOK, J. A. FENDRICH, C. J. VAN DER BEEK, and G. W. CRABTREE, *Phys. Rev. Lett.* **73**, 2614 (1994).

[22] M. TINKHAM, *Introduction to superconductivity*, volume 89, McGraw-Hill New York, 1975.

[23] J. PEARL, *Applied Physics Letters* **5**, 65 (1964).

[24] E. ZELDOV, N. M. AMER, G. KOREN, A. GUPTA, R. J. GAMBINO, and M. W. MCELFRESH, *Phys. Rev. Lett.* **62**, 3093 (1989).

[25] E. ZELDOV, N. AMER, G. KOREN, A. GUPTA, M. MCELFRESH, and R. GAMBINO, *Applied physics letters* **56**, 680 (1990).

[26] V. AMBEGAOKAR and B. I. HALPERIN, *Phys. Rev. Lett.* **22**, 1364 (1969).

[27] M. TINKHAM, *Phys. Rev. Lett.* **61**, 1658 (1988).